IOP Publishing Semiconductor Science and Technology
Semicond. Sci. Technol. **33** (2018) 055006 (8pp) https://doi.org/10.1088/1361-6641/aab8a6

Current Transport Properties of Monolayer Graphene/n-Si Schottky Diodes

C S Pathak[1], Manjari Garg, J P Singh[1] and R Singh

Department of Physics, Indian Institute of Technology Delhi, Hauz Khas, New Delhi-110016, India

E-mail: cspathak12@physics.iitd.ac.in and jpsingh@physics.iitd.ac.in

Received 28 December 2017, revised 16 March 2018
Accepted for publication 22 March 2018
Published 16 April 2018

Abstract

The present work reports on the fabrication and the detailed macroscopic and nanoscale electrical characteristics of monolayer graphene/*n*-Si Schottky diodes. The temperature dependent electrical transport properties of monolayer graphene/*n*-Si Schottky diodes were investigated. Nanoscale electrical characterizations were carried out using Kelvin probe force microscopy and conducting atomic force microscopy. Most the values of ideality factor and barrier height are found to be in the range of 2.0–4.4 and 0.50–0.70 eV for monolayer graphene/*n*-Si nanoscale Schottky contacts. The tunneling of electrons is found to be responsible for the high value of ideality factor for nanoscale Schottky contacts.

Keywords: electrical, nanoscale, graphene, KPFM, CAFM

(Some figures may appear in colour only in the online journal)

1. Introduction

In recent years, graphene, which is a two-dimensional (2D) single-atom carbon sheet has attracted great attention due to its unique and novel electronic, optical and mechanical properties alongside its thermal and chemical stability [1]. Graphene has been grown in the form of ultrathin sheets, consisting of single or few layers, by chemical vapor deposition (CVD) [2], solution processing [3], and the micromechanical exfoliation of graphite [4]. CVD grown graphene has a large surface area, which is an advantage over exfoliated graphene. CVD grown graphene can easily be transferred on to the required substrates. CVD graphene has the high electrical conductivity and optical transmittance required for optoelectronic applications [5]. The CVD graphene transfer process is cheap and it does not require high temperatures. Previously, the Schottky barrier has been reported for graphene and for various semiconductors such as Si [2, 6–13], GaAs [7, 14], SiC [7, 15], and GaN [16–19]. The extraordinary properties of graphene make it a promising material for future high-speed electronics, optoelectronics, photovoltaics, photodetectors and sensors [9, 14, 20–23]. Therefore, the investigation of Schottky contacts between graphene and various semiconductors is an important topic in graphene based devices as it is important to understand the interface between graphene and various metals or semiconductors. Previously published works related to Schottky diodes based on graphene have focused on the electrical and optical characteristics, but the fundamental transport mechanism is not properly understood. The analysis of current-voltage (I-V) characteristics of a Schottky diode at room temperature does not provide sufficient information about the transport mechanisms. For a better understanding of the transport mechanisms of the fabricated devices, we have assessed the temperature dependence of I-V characteristics of monolayer graphene/Si Schottky diode. Conventionally graphene based semiconductor devices have been studied using macroscopic techniques. In order to study localized behavior, analysis can be performed directly at the area of interest with the help of scanning probe microscopy (SPM), which provides high resolution imaging and localized electrical measurements at nanoscale dimensions.

In this work, we report on the current transport properties of monolayer graphene/*n*-Si Schottky diodes. To understand the transport mechanism, temperature dependent I-V measurements were carried out. Kelvin probe force microscopy (KPFM) and conducting atomic force microscopy (CAFM) measurements were performed to investigate the nanoscale electrical properties of monolayer graphene/*n*-Si Schottky diodes. To the best of our knowledge, comparison of transport

[1] Authors to whom any correspondence should be addressed.

mechanisms for macroscopic and nanoscale electrical properties of monolayer graphene/*n*-Si Schottky diodes has not been reported. The analysis of the temperature dependent transport properties and nanoscale electrical properties are important for future electronic devices.

2. Experimental

CVD grown monolayer graphene was purchased from log9 Materials, India. Silicon (*n*-type) wafers (100) were cleaned in an ultrasonic bath to get the surface free from contamination. Successive treatments in acetone, isopropanol and deionized (DI) water were carried out at laboratory temperature. Poly methyl methacrylate (PMMA) was spin coated on the Cu foil at 2000 rpm for 60 s and then the sample was baked at 180 °C for 2 min on a hot plate. PMMA coated graphene/Cu samples were placed in ferric chloride solution to etch Cu. After the removal of Cu, PMMA coated graphene was cleaned thoroughly using DI water for 20 min. Finally, PMMA coated graphene was transferred onto the thermally oxidized Si samples with oxide layer thickness of about 300 nm and having 60 nm thick aluminum metal. To remove the PMMA layer, the transferred graphene samples were immersed in acetone for 2 h followed by cleaning with DI water and isopropyl alcohol several times and finally dried at room temperature.

Raman spectra of graphene samples were obtained using Raman spectroscopy (Horiba LabRAM HR). Surface potential was measured using Kelvin probe atomic force microscopy (KPFM) (Bruker Dimension Icon) in tapping mode. The nanoscale current voltage (*I-V*) characteristics were taken with the help of CAFM in contact mode. Macroscopic (*I-V*) measurements were performed using Keithley's semiconductor characterization system (SCS-4200) and a temperature controller Cryocon (Model 32) from low temperature 100 to 200 K. EverBeing DC probe station was used for high temperature measurements from room temperature (RT) 300 to 373 K.

3. Results and discussion

The CVD grown graphene was transferred on to SiO_2/Si substrates for Schottky junction formation. Figure 1 shows the Raman spectra of graphene after transfer onto SiO_2/Si substrate. The intensity ratio of I_{2D}/I_G is 3.5 and 2*D* peak at about 2685 cm^{-1} with a half peak width of 36 cm^{-1} imply that the graphene film on Si substrate was a monolayer, which is in good agreement with the values reported in the previous reports for monolayer graphene [10]. The presence of *D* peak at 1345 cm^{-1} indicates the presence of defects which might happen due to the transfer process of graphene [11].

The KPFM measurements were used to record images of monolayer graphene surface topography and contact potential difference (CPD) between the conducting Pt-Ir tip and graphene surface. It is well known that KPFM results can be affected by environmental changes such as moisture and tip

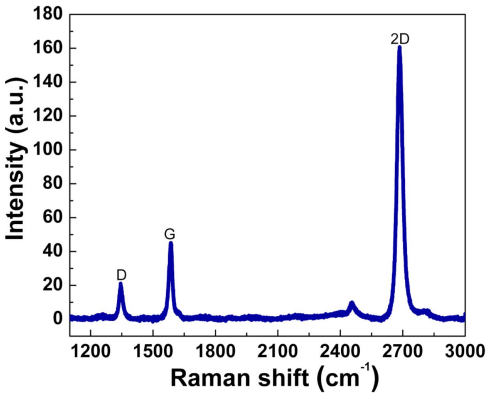

Figure 1. Raman spectra of graphene on SiO_2/Si substrate.

conditions. Therefore to achieve reproducible results the surface potential of graphene was measured at various places using the same tip. The average value of surface potential was used to calculate the work function of monolayer graphene according to the following equation [24],

$$V_{CPD} = \frac{\phi_{tip} - \phi_{sample}}{-q} \quad (1)$$

where V_{CPD} is the contact potential different measured by KPFM in volts, ϕ_{tip}, ϕ_{sample} are the work functions of tip and sample in eV, respectively and q is the electronic charge. Silicon tips coated with conductive Pt-Ir and a nominal radius of curvature of 25 nm were used to perform KPFM measurements. The spring constant and resonant frequency of these tips were 2.8 N m^{-1} and 75 kHz, respectively. Figure 2(a) shows the schematic representation of KPFM measurements and figures 2(b) & (c) show surface potential images of highly oriented pyrolytic graphite (HOPG) and grapheme, respectively.

The value of ϕ_{tip} was obtained by calibration with respect to freshly cleaved HOPG. The value of ϕ_{sample} for HOPG was taken as 4.6 eV [25, 26]. The average value of surface potential of HOPG was found to be 360 mV, which gives the estimated mean value of ϕ_{tip} as 4.96 eV. The average value of surface potential of graphene was measured as 417 mV which gives the average work function of graphene as 4.54 eV. Panchal *et al* [27] have measured work function value of monolayer graphene using the KPFM technique and they found the work function value of monolayer graphene to be 4.55 eV.

Before the transfer of monolayer graphene on Al/SiO_2/Si surface, an open circuit is observed between the Al pad and ohmic contact. After the transfer of the graphene, an electrical connection is self-established between the graphene/Al and graphene/*n*-Si. To understand the transport mechanisms, we have studied the temperature dependent *I-V* characteristics of monolayer graphene/*n*-Si Schottky diodes, as shown in figure 3(a). It can be seen that the current rectification at ±1 V increases with the decrease in temperature. For thermionic emission (TE) and $V > 3kT/q$, the general

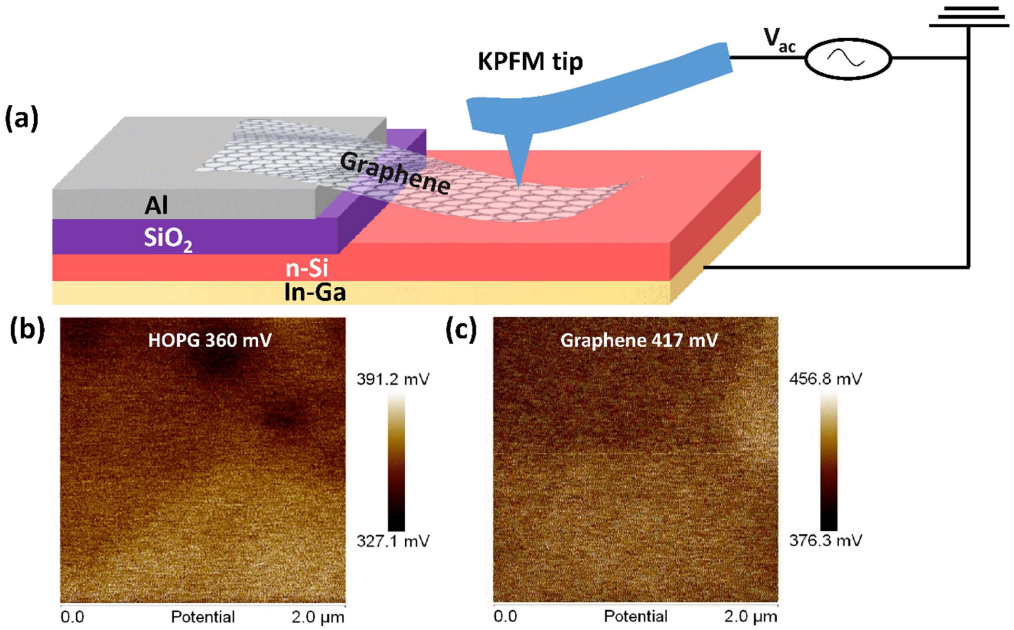

Figure 2. (a) Schematic representation of KPFM measurements (figure not to scale), and (b) & (c) show surface potential image of HOPG and graphene, respectively.

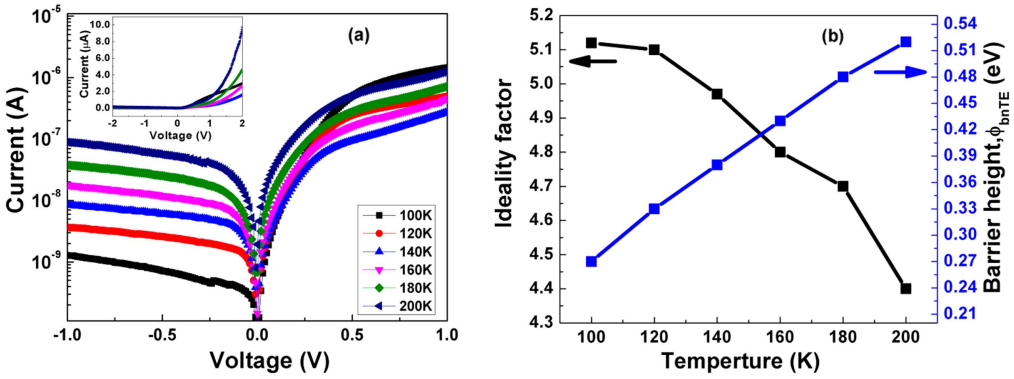

Figure 3. (a) Semi-log forward and reverse *I-V* characteristics, and (b) apparent barrier height and ideality factor vs. temperature plot for graphene/*n*-Si Schottky diode.

diode equation is [28],

$$I_n = \left[AA^*T^2 \exp\left(-\frac{q\phi_{bnTE}}{kT}\right)\right]\left[\exp\left(\frac{qV}{\eta kT}\right) - 1\right] \tag{2}$$

where A is the area of the Schottky diode, A* is the effective Richardson coefficient, T is the absolute temperature, q is the fundamental electronic charge, ϕ_{bnTE} is the barrier height, k is the Boltzmann's constant, V is the applied voltage and η is the ideality factor. From the forward bias log I versus V plot, ideality factor η and barrier height ϕ_{bnTE} were calculated from the slope and intercept of the linear region, respectively at different temperatures in the range of 200–100 K. Using equation (2), the values of ideality factor and barrier height of the diode at different temperatures were calculated and are plotted as a function of temperature in figure 3(b).

Since $\eta > 1$, the *I-V* behavior apparently deviates from the TE model in the forward bias region. In order to explain the observed temperature dependence of *I-V* behavior of the monolayer graphene/*n*-Si Schottky interface a tunneling transport mechanism based thermionic field-emission (TFE) model was provoked [29]. Under forward bias, the current due to TFE and for $V_F > kT/q$ is given by

$$I_{TFE} = \frac{AA^*T\sqrt{\pi E_{oo} q(\phi_{bnTFE} - \phi_n - V_F)}}{k\cos h(E_{oo}/kT)} \times \exp\left[\frac{-q\phi_n}{kT} - \frac{q(\phi_{bnTFE} - \phi_n)}{E_o}\right] exp\left(\frac{qV_F}{E_o}\right) \tag{3}$$

$$E_{oo} = \frac{q\hbar}{2}\sqrt{\frac{N}{m^*\epsilon_s}}, \qquad E_o = E_{oo}\coth\left(\frac{E_{oo}}{kT}\right) \tag{4}$$

where V_F is the forward bias voltage, ϕ_n is E_C—E_F, ϕ_{bnTFE} is the Schottky barrier height, h is the Planck's constant, N is the donor density, m^* is the effective mass and ϵ_s is the dielectric constant. E_{oo} is the characteristic energy related to the tunneling probability of a triangular potential barrier using the WKB approximation. From the forward bias log I versus V plot, barrier height ϕ_{bnTFE} was calculated at different temperatures in the range of 200–100 K, using equations (3) and

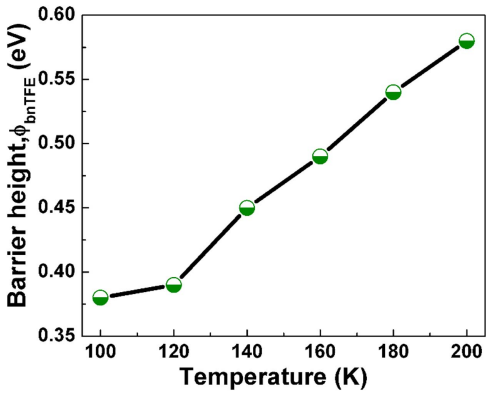

Figure 4. Barrier height variations with temperature obtained by using thermionic field emission.

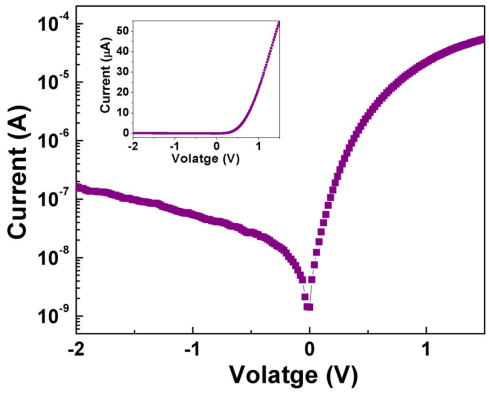

Figure 5. Room temperature *I-V* characteristics of graphene/*n*-Si Schottky diode.

(4) and the calculated barrier height as a function of temperature is shown in figure 4.

Figure 5 shows the RT *I-V* characteristics of monolayer graphene/*n*-Si Schottky diode. At RT the value of ideality factor and barrier height were found to be 2.0 and 0.84 eV, respectively. The obtained values of ideality factor and barrier height at RT are in good agreement with the earlier reported values. Parui *et al* [12] have fabricated CVD graphene/*n*-Si Schottky diodes and the values of ideality factor and barrier height were found as 2.53 and 0.83 eV, respectively. In another research the value of barrier height of 0.79 eV was obtained for graphene/*n*-Si diode [27]. Wang *et al* [13] have fabricated CVD graphene/Si Schottky junction and observed the value of ideality factor as 1.75 and barrier height as 0.81 eV.

Figure 6(a) shows the *I-V* characteristics of graphene/*n*-Si Schottky diodes at high temperature. The values of ideality factor and barrier height of the diode at higher temperatures were calculated and are plotted as a function of temperature in figure 6(b). At 100 °C there was a decrease in current value and the ideality factor is higher than that at RT which may be due to the oxidation of Al. At higher temperatures $\eta > 1$ suggests that the TE may not be the dominant current transport mechanism, TFE and tunneling might be the dominant current transport mechanisms.

The Schottky barrier height (SBH) versus ideality factor (IF) plot has been presented in figure 7. The extrapolation of the experimental barrier heights versus ideality factor plot to $\eta = 1$ gives the value of homogeneous barrier height of approximately 0.993 eV. The other barrier height values deviate from this value due to local inhomogeneities.

The Schottky barrier inhomogeneity can be explained with the help of the Werner model [30]. According to this model there is a Gaussian distribution of SBH at the inhomogeneous metal-semiconductor interface. The SBHs are distributed around a mean value $\overline{\phi_{bo}}$ with a standard deviation σ_s. Consequently, the SBH varies with temperature which is mathematically expressed as:

$$\phi_{bo} = \overline{\phi_{bo}} - \frac{\sigma_s^2}{2kT} \tag{5}$$

According to the equation, a plot between ϕ_{bo} (in eV) and $2kT^{-1}$ (in eV^{-1}) should yield a straight line with slope giving the value of σ_s and y-intercept giving the value of $\overline{\phi_{bo}}$. For the graphene-Si interface, the values of $\overline{\phi_{bo}}$ and σ_s are calculated as 0.77 eV and 91.3 meV, respectively which quantifies the Schottky barrier inhomogeneity, as shown in figure 8.

The variation of ideality factor with temperature is given by

$$\eta = \frac{1}{1 - \rho_2 + \frac{q\rho_3}{2kT}} \tag{6a}$$

In this expression ρ_2 and ρ_3 quantify the deformation of the barrier distribution with the applied voltage. ρ_2 is the sensitivity of the mean barrier height variation to the field and ρ_3 is the sensitivity of the barrier height standard deviation variation to the field according to

$$\rho_2 V = \overline{\phi_b}(V) - \overline{\phi_{bo}} \quad \text{and} \quad \rho_3 V = \sigma_s^2(V) - \sigma_o^2 \tag{6b}$$

A plot between $\eta^{-1} - 1$ and $2kT^{-1}$ (in eV^{-1}) should yield a straight line with slope giving the value of ρ_2 and y-intercept giving the value of ρ_3. For our case, ρ_2 and ρ_3 are calculated as −0.75 and −0.992 meV, respectively, as shown in figure 8.

The localized *I-V* behavior was studied using CAFM. The mapping of the current on the surfaces gives the direct information of electrical properties at nanoscale dimensions. Local *I-V* characteristics were found by using an AFM equipped with a high sensitivity current amplifier in series with CAFM tip, which acts as a nanometric metal contact over the sample surface. Local *I-V* measurements were carried out at random locations using a Pt-Ir tip. The bias was applied between the Pt-Ir tip and a macroscopic ohmic contact of In-Ga fabricated on the back side of the Si substrate. A map of the current flowing from tip to graphene surface was collected. Figure 9(a) shows the schematic representation of CAFM measurements and figure 9(b) shows the CAFM current map under a constant bias. The maximum current obtained was 12.3 nA. Local *I-V* characteristics were recorded at random locations to analyze the localized variations in ideality factor and barrier height. Figure 9(c) shows the typical *I-V* curve obtained from CAFM and during the CAFM analysis. 30 such *I-V* curves have been collected at different randomly selected locations on the sample with the Pt-Ir tip.

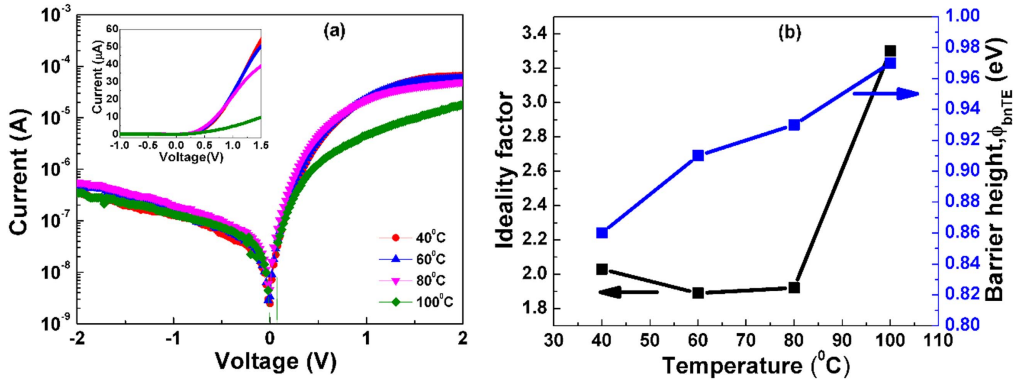

Figure 6. (a) Semi-log forward and reverse *I-V* characteristics, and (b) apparent barrier height and ideality factor vs. temperature plot for graphene/*n*-Si Schottky diode.

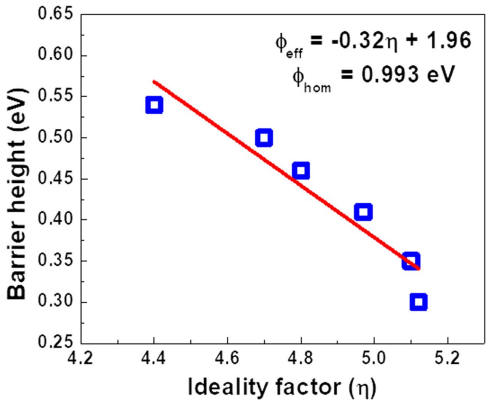

Figure 7. Variation of experimentally calculated Schottky barrier height with ideality factor.

From all local *I-V* curves collected from random locations using the Pt-Ir tip, values of ideality factor and barrier height were determined. Leroy *et al* [31] used a conducting probe atomic force microscope and measured an average barrier height of the whole contact (μm scale) instead of local nanometer-scale barrier heights for Au/n-GaAs Schottky barrier diodes.

For nanoscale Schottky contacts the ideality factor values range from between 2 to 4. For nanoscale contact the Schottky barrier height can be considered as homogeneous within the contact area, and surface states, tunneling, electrical dipole formation etc are responsible for an ideality factor >1. The role of barrier inhomogeneities will be less due to the nanoscale dimensions contact area between the Pt-Ir tip and sample surface [32, 33]. At nanoscale dimensions the properties of diodes deviate significantly because of the tunneling current which becomes significant for diode size less than or comparable with the zero bias depletion width [34]. Zero bias depletion width (δ) can be calculated as:

$$\delta = \sqrt{\frac{2\varepsilon(\phi_{bn} - \xi)}{q^2 N_D}} \tag{7}$$

Here ϕ_{bn} is Schottky barrier height, $\xi = KT \ln\left(\frac{N_c}{N_D}\right)$, where N_C is equal to $2.8 \times 10^{19}\,\mathrm{cm}^{-3}$, N_D is doping concentration equal to $2 \times 10^{18}\,\mathrm{cm}^{-3}$ in Si from Hall measurements and $\varepsilon = 11.7\varepsilon_o$ is the permittivity of Si. By taking $\phi_{bn} = 0.60$ eV, δ is calculated as 19 nm and the radius of curvature of tip is 25 nm, which is comparable with δ. Therefore, tunneling current could become significant at nanoscale interface causing deviation of the ideality factor from unity.

To calculate the Schottky barrier height of the nanosize contact, the area of CAFM tip in contact with the graphene is required. Hence, effective area (A_{eff}) of contact between the tip and the graphene is calculated using the Hertz contact model [34]. According to this model, two spherical bodies make a circular contact with radius (r) under the effect of normal force. The two bodies in contact are CAFM tip and the graphene surface. The expressions for r and A_{eff} are given as [35],

$$r = \left(\frac{3PR}{4E^*}\right)^{1/3} \tag{8}$$

$$A_{eff} = \pi r^2 = \pi\left(\frac{3PR}{4E^*}\right)^{2/3} \tag{9}$$

where P is the normal load, R is the relative radius of curvature, E^* is the contact modulus, v is the Poisson's ratio and E is the Young's modulus.

$$\frac{1}{R} = \frac{1}{R_{tip}} + \frac{1}{R_{sample}} \tag{10}$$

$$\frac{1}{E^*} = \frac{1 - \nu_{tip}^2}{E_{tip}} + \frac{1 - \nu_{sample}^2}{E_{sample}} \tag{11}$$

where E_{tip}, E_{sample}, υ_{tip} and υ_{sample} are Young's modulus and the Poisson ratios of sample and tip. By using this model, we obtained the area about 25 nm^2. Using equation (2), we obtained the value of barrier height using the nanometric tip. For nanoscale Schottky contacts the barrier height values ranges between 0.50–0.70 eV. For nanoscale contacts, the Schottky barrier height can be considered as homogeneous within the contact area and hence, inhomogeneities are not expected to affect the current transport at nanoscale dimensions.

The energy band diagram of monolayer graphene/*n*-Si is shown in figure 10. As shown in schematic diagrams, graphene is in contact with Al as well as with Si. The Fermi level shifts due to the metal surface which causes the electron and

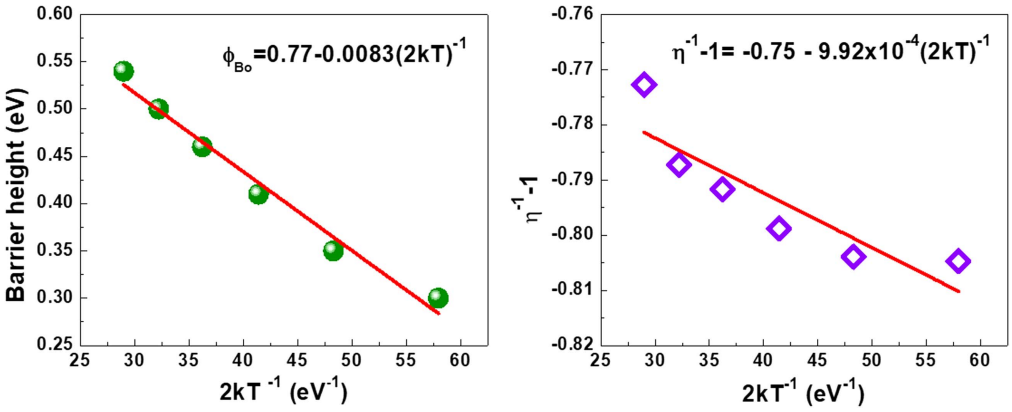

Figure 8. Temperature dependent plots of barrier height and ideality factor to quantify the barrier height inhomogeneity at the graphene-Si semiconductor interface.

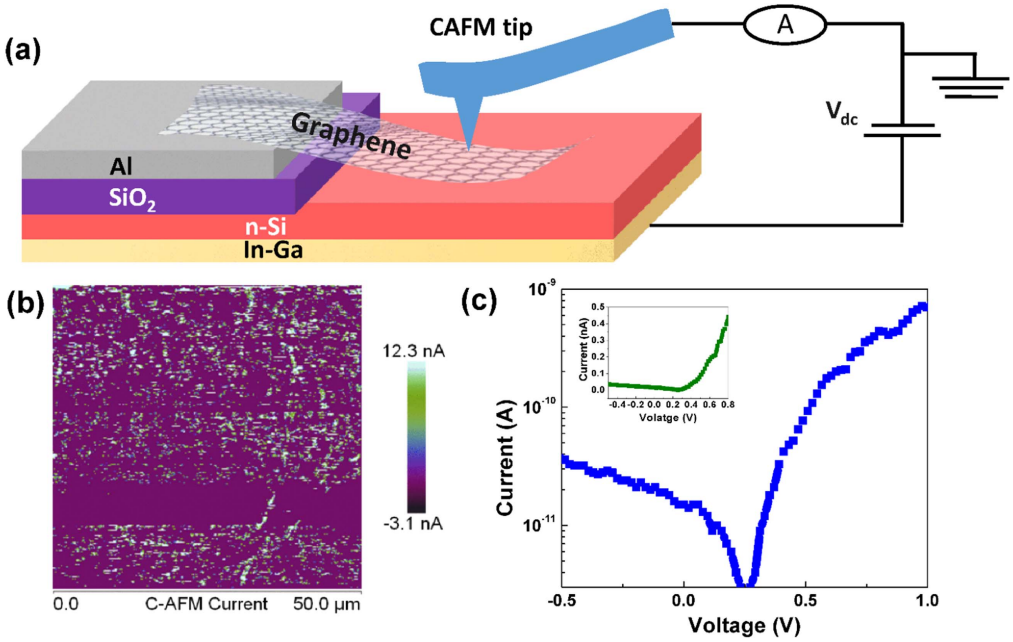

Figure 9. (a) Schematic representation of CAFM measurements (figure not to scale), (b) current image of graphene, and (c) CAFM *I-V* characteristics of graphene/*n*-Si Schottky diode.

hole doping in graphene [36, 37]. The shifting of the Fermi level depends upon the work function of the metal surface and graphene. If the work function of the metal surface is less than the work function of graphene then electrons move from metal to graphene and results in electron doping in the graphene. If the work function of the clean metal surface is greater than the work function of graphene then electrons move from graphene to metal and results in hole doping in the graphene. The average value of the work function (Φ_G) for graphene is 4.54 eV as measured by KPFM. The work function of Al is taken as 4.26 eV [28] and due to the work function difference between Al and graphene, electron moves from Al to graphene and hence, results in electron doping in graphene.

4. Conclusions

In summary, we have fabricated CVD grown monolayer graphene/*n*-Si Schottky diodes and studied temperature dependent *I-V* measurements to investigate the transport. Temperature dependent *I-V* measurements show a decrease in barrier height and an increase in ideality factor with increases in the sample temperature. Nanoscale CAFM analysis was employed to investigate the electrical properties of the diodes at nanoscale to evaluate the localized ideality factor and barrier height of the device. The CAFM analysis shows that a nanoscale Schottky contact was formed between CAFM tip and the sample surface. Tunneling was found to be the dominant current transport mechanism at nanoscale.

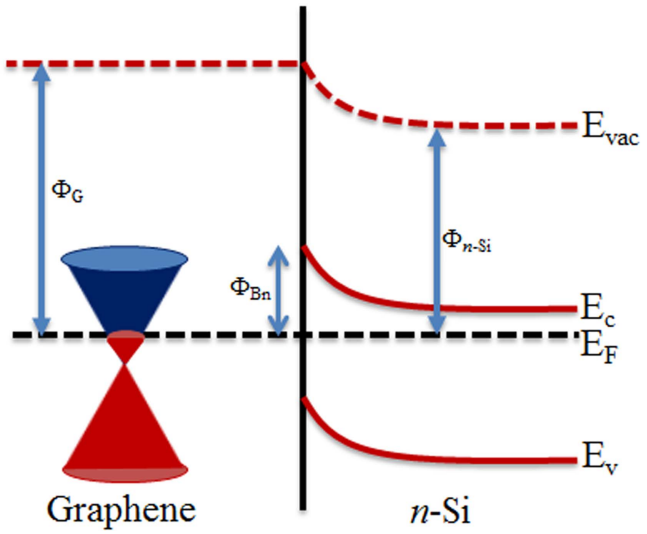

Figure 10. Energy band diagram of graphene/*n*-Si Schottky diode.

Acknowledgments

One of the authors (CSP) acknowledges IIT Delhi for providing senior research fellowship. The authors acknowledge Nanoscale Research Facility (NRF) at IIT Delhi for providing the electrical characterization facilities and SERB, DST, India (project No. EMR/2015/001477).

ORCID iDs

C S Pathak https://orcid.org/0000-0003-0718-4749
R Singh https://orcid.org/0000-0002-6890-6904

References

[1] Liu X, Zhang X W, Yin Z G, Meng J H, Gao H L, Zhang L Q, Zhao Y J and Wang H L 2014 Enhanced efficiency of graphene-silicon Schottky junction solar cells by doping with Au nanoparticles *Appl. Phys. Lett.* **105** 183901
[2] Chen C, Aykol M, Chang C, Levi A F J and Cronin S B 2011 Graphene-silicon schottky diodes *Nano Lett.* **11** 1863–7
[3] Li X, Zhang G, Bai X, Sun X, Wang X, Wang E and Dai H 2008 Highly conducting graphene sheets and Langmuir–Blodgett films *Nat. Nanotechnol.* **3** 538–42
[4] Tang Z, Zhuang J and Wang X 2010 Exfoliation of graphene from graphite and their self-assembly at the oil-water interface *Langmuir* **26** 9045–9
[5] Reina A, Jia X, Ho J, Nezich D, Son H, Bulovic V, Dresselhaus M S and Jing K 2009 Large area, few-layer graphene films on arbitrary substrates by chemical vapor deposition *Nano Lett.* **9** 30–5
[6] Sinha D and Lee J U 2014 Ideal graphene/silicon schottky junction diodes *Nano Lett.* **14** 4660–4
[7] Tongay S, Schumann T and Hebard A F 2009 Graphite based Schottky diodes formed on Si, GaAs, and 4H-SiC substrates *Appl. Phys. Lett.* **95** 4–7
[8] Yim C, McEvoy N and Duesberg G S 2013 Characterization of graphene-silicon Schottky barrier diodes using impedance spectroscopy *Appl. Phys. Lett.* **103** 193106 –5
[9] Li X, Zhu H, Wang K, Cao A, Wei J, Li C, Jia Y, Li Z, Li X and Wu D 2010 Graphene-on-silicon schottky junction solar cells *Adv. Mater.* **22** 2743–8
[10] Ruan K, Ding K, Wang Y, Diao S, Shao Z, Zhang X and Jie J 2015 Flexible graphene/silicon heterojunction solar cells *J. Mater. Chem.* A **3** 14370–7
[11] Kumar R, Varandani D and Mehta B R 2016 Nanoscale interface formation and charge transfer in graphene/silicon Schottky junctions; KPFM and CAFM studies *Carbon N. Y.* **98** 41–9
[12] Parui S, Ruiter R, Zomer P J, Wojtaszek M, Van Wees B J and Banerjee T 2014 Temperature dependent transport characteristics of graphene/n-Si diodes *J. Appl. Phys.* **116** 1–6
[13] Wang X, Wang Y, Li D, Zou L, Zhang Q, Zhou J, Liu D and Zhang Z 2015 Thermal annealing and air exposing effect on the graphene/silicon Schottky junctions *Solid State Commun.* **201** 115–9
[14] Jie W, Zheng F and Hao J 2013 Graphene/gallium arsenide-based Schottky junction solar cells *Appl. Phys. Lett.* **103** 233111–4
[15] Shivaraman S, Herman L H, Rana F, Park J and Spencer M G 2012 Schottky barrier inhomogeneities at the interface of few layer epitaxial graphene and silicon carbide *Appl. Phys. Lett.* **100** 18112–4
[16] Tongay S, Lemaitre M, Schumann T, Berke K, Appleton B R, Gila B and Hebard A F 2011 Graphene/GaN Schottky diodes: stability at elevated temperatures *Appl. Phys. Lett.* **99** 102102–3
[17] Kim S, Seo T H, Kim M J, Song K M, Suh E K and Kim H 2015 Graphene-GaN Schottky diodes *Nano Res.* **8** 1327–38
[18] Tongay S, Lemaitre M, Miao X, Gila B, Appleton B R and Hebard A F 2012 Rectification at graphene-semiconductor interfaces: Zero-gap semiconductor-based diodes *Phys. Rev.* X **2** 1–10
[19] Kumar A, Kashid R, Ghosh A, Kumar V and Singh R 2016 Enhanced thermionic emission and low 1/f noise in exfoliated graphene/GaN Schottky barrier diode *ACS Appl. Mater. Interfaces* **8** 8213–23
[20] Castro Neto A H, Guinea F, Peres N M R, Novoselov K S and Geim A K 2009 The electronic properties of graphene *Rev. Mod. Phys.* **81** 109–62
[21] Withers F, Bointon T H, Craciun M F and Russo S 2013 All-graphene photodetectors *ACS Nano* **7** 5052–7
[22] Miao X, Tongay S, Petterson M K, Berke K, Rinzler A G, Appleton B R and Hebard A F 2012 High efficiency graphene solar cells by chemical doping *Nano Lett.* **12** 2745–50
[23] Shao Y, Wang J, Wu H, Liu J, Aksay I A and Lin Y 2010 Graphene based electrochemical sensors and biosensors: A review *Electroanalysis* **22** 1027–36
[24] Melitz W, Shen J, Kummel A C and Lee S 2011 Kelvin probe force microscopy and its application *Surf. Sci. Rep.* **66** 1–27
[25] Melitz W, Shen J, Lee S, Lee J S, Kummel A C, Droopad R and Yu E T 2010 Scanning tunneling spectroscopy and Kelvin probe force microscopy investigation of Fermi energy level pinning mechanism on InAs and InGaAs clean surfaces *J. Appl. Phys.* **108** 023711–7
[26] Beerbom M M, Lägel B, Cascio A J, Doran B V and Schlaf R 2006 Direct comparison of photoemission spectroscopy and in situ Kelvin probe work function measurements on indium tin oxide films *J. Electron Spectros. Relat. Phenomena* **152** 12–7
[27] Panchal V, Pearce R, Yakimova R, Tzalenchuk A and Kazakova O 2013 Standardization of surface potential measurements of graphene domains *Sci. Rep.* **3** 2597–8
[28] Sze S M and Ng K K 2007 *Physics of Semiconductor Devices* (Hoboken, NJ: Wiley-Interscience)

[29] Padovani F A and Stratton R 1966 Field and thermionic-field emission in Schottky barriers *Solid. State. Electron.* **9** 695–707
[30] Werner J H and Güttler H H 1991 Barrier inhomogeneities at Schottky contacts *J. Appl. Phys.* **69** 1522–33
[31] Leroy W P, Opsomer K, Forment S and Van Meirhaeghe R L 2005 The barrier height inhomogeneity in identically prepared Au/n-GaAs Schottky barrier diodes *Solid. State. Electron.* **49** 878–83
[32] Kumar A, Heilmann M, Latzel M, Kapoor R, Sharma I, Göbelt M, Christiansen S H, Kumar V and Singh R 2016 Barrier inhomogeneities limited current and 1/f noise transport in GaN based nanoscale Schottky barrier diodes *Sci. Rep.* **6** 27553
[33] Kumar A, Kapoor R, Garg M, Kumar V and Singh R 2017 Direct evidence of barrier inhomogeneities at metal/AlGaN/GaN interfaces using nanoscopic electrical characterizations *Nanotechnology* **28** 26LT02
[34] Smit G D J, Rogge S and Klapwijk T M 2002 Scaling of nano-Schottky-diodes *Appl. Phys. Lett.* **81** 3852–4
[35] Johnson K L, Kendall K and Roberts A D 1971 Surface energy and the contact of elastic solids *Proc. R. Soc. A Math. Phys. Eng. Sci.* **324** 301–13
[36] Giovannetti G, Khomyakov P A, Brocks G, Karpan V M, Van Den Brink J and Kelly P J 2008 Doping graphene with metal contacts *Phys. Rev. Lett.* **101** 3–6
[37] Khomyakov P A, Giovannetti G, Rusu P C, Brocks G, Van Den Brink J and Kelly P J 2009 First-principles study of the interaction and charge transfer between graphene and metals *Phys. Rev. B—Condens. Matter Mater. Phys.* **79** 1–12